A numerical study on the effects of cavitation on orifice flow

S. Dabiri,[1] W. A. Sirignano,[1] and D. D. Joseph[1,2]
[1]*University of California, Irvine, California 92697, USA*
[2]*University of Minnesota, Minneapolis, Minnesota 55455, USA*

(Received 31 July 2009; accepted 11 March 2010; published online 21 April 2010)

Previous experimental studies have shown better atomization of sprays generated by high-pressure liquid injectors when cavitation occurs inside the nozzle. It has been proposed that the collapse of traveling cavitation bubbles increases the disturbances inside the liquid flow. These disturbances will later trigger the instabilities in the emerged jet and cause a shorter breakup distance. In this paper, effects of cavitation on increasing the disturbances in the flow through the orifice of an atomizer are studied. In previous cavitation models, spherical cavitation bubbles are considered. Here, the cavitation bubbles are allowed to deform as they travel through the orifice. Dynamics of the cavitation bubble, traveling in the separated shear layer in the orifice, is analyzed through a one-way coupling between the orifice flow and bubble dynamics. Effects of shear strain, normal strain, and pressure variation are examined. Three mechanisms are suggested that could be responsible for the increase in disturbances in the flow due to cavitation. These mechanisms are monopole, quadrupole, and vorticities generated during growth and collapse of cavitation bubbles. The effects of these mechanisms are estimated by postprocessing of the solutions to the Navier–Stokes equations to identify monopole and quadrupole behaviors. © *2010 American Institute of Physics*. [doi:10.1063/1.3386014]

I. INTRODUCTION

High-pressure atomizers and spray generators are of great interest in industry and have many applications such as liquid fuel injectors, drying systems, and agricultural sprays. Experiments have shown that occurrence of cavitation in high-pressure liquid injectors leads to a better atomization of the emerged jet.[1,2] It has been proposed that the collapse of traveling cavitation bubbles increases the disturbances inside the liquid flow. These disturbances later will trigger the natural instabilities in the emerged jet, and cause a shorter breakup distance. In an experiment, He and Ruiz[3] observed that when cavitation is present in an orifice flow, the turbulence intensity is much higher than the flow without cavitation but with same Reynolds number. Effects of cavitation on atomization have been studied by Arcoumanis *et al.*[4,5] and more recently by Andriotis *et al.*[6] Different models for cavitation have been proposed that provide good results for vapor fraction and velocity profiles inside the nozzle.[7,8] However, the effects of cavitation on the jet breakup has not been fully understood. Kubota[9] developed a model for cavitating flows in which the cavitation cloud is considered as a local homogenous cluster of spherical bubbles. Then, through a mean-field theory, the governing equation for the rate of change of the radius of the bubbles is calculated from the Rayleigh–Plesset–Poritsky equation. Giannadakis *et al.*[8] also employed the approach of Kubota to extend the bubble dynamics to a cluster of bubbles. They simulated the cavitation in a diesel nozzle hole.

The cavitation models developed by Kubota[9] and others[8] are based on the assumption of spherical cavitation bubbles and the effects of deformation of bubbles have not been considered. In this paper, effects of cavitation bubbles on the velocity field are investigated to find the mechanisms that are responsible for the increase in the disturbances in the flow. In addition, the deformation of the cavitation bubbles are resolved which will be helpful in understanding the other contributions of the cavitation bubble to the velocity field in addition to the volume change, modeled by spherical bubbles.

Depending on the cavitation number, the flow could show no cavitation, cavitation with traveling bubbles, cavitation with a fixed vapor bubble behind the corner, or supercavitation. Attempts to predict susceptibility to stress-induced cavitation in high-pressure orifice flows have been advanced by Dabiri *et al.*[10,11] The analysis indicates that cavitation is most likely in the regions of high shear stress. Therefore, it is important to study cavitation bubbles in such environments. Note that Refs. 4–8 did not consider stress-induced cavitation.

Yu *et al.*[12] studied the collapse of a cavitation bubble inside a boundary layer over a rigid wall. They observed that for sufficiently large shear the collapse rate of the bubble will increase and the reentrant jet will disappear. Experiments also have shown that the high shear stress can cause cavitation in the liquid even at high pressures. For example, Kottke *et al.*[13] observed cavitation in creeping flow at pressures much higher than the vapor pressure.

Dabiri *et al.*[14] studied the growth and collapse of cavitation bubbles in shear flow and extensional flow. It has been observed that combination of pressure variation and a shear results in large deformation of bubbles and even breakup of the cavitation bubbles.

All of the previous works on modeling the cavitating liquid injectors considered the flow to be either a pseudo-single phase with continuous density variation and without specification of bubble characteristics or a liquid phase with

spherical cavitation bubbles traveling in the liquid. In this work, we study the deformation of cavitation bubbles and their effects on a flow through the orifice of an atomizer. We are focused on stress-induced cavitation and therefore consider bubbles that move through the shear layer near the wall.

This work is a result of a one-way coupling. We are examining the effect of the bubble growth and collapse on generating turbulence. We are not considering a flow with developed turbulence due to cavitation. First, we discuss the Navier–Stokes solution of the orifice flow. Then, the pressure variation and shear stress inside the orifice are extracted and used to create a similar environment for a cavitation bubble. Bubble dynamics is analyzed using the same approach as Dabiri *et al.*[14] Finally, the disturbances caused by this cavitation bubble on the free jet emerging from the nozzle are estimated.

II. GOVERNING EQUATIONS AND NUMERICAL METHOD

We consider the deformation of a cavitation bubble in a viscous liquid flowing through a short orifice. Although the Reynolds number based on diameter may be large the flow will be transitional and will be considered as unsteady, laminar. The governing equations for this three-dimensional problem follow

$$\rho_i\left(\frac{\partial \mathbf{u}}{\partial t}+\mathbf{u}\cdot\nabla\mathbf{u}\right)=-\nabla p+\nabla\cdot\mathbf{T}+\sigma\kappa\delta(d)\mathbf{n}, \tag{1}$$

where $\mathbf{u}$, ρ, and μ are the velocity, density, and viscosity of the fluid, respectively. Subscript i could represent either liquid (l) or gas (g) phase and $\mathbf{T}$ is the viscous stress tensor. The last term represents the surface tension as a force concentrated on the interface. Here, σ is the surface tension coefficient, κ is twice the local mean curvature of the interface, δ is the Dirac delta function, d represents the distance from the interface, and $\mathbf{n}$ corresponds to the unit vector normal to the interface. The continuity equation for the liquid is

$$\nabla\cdot\mathbf{u}=0, \tag{2}$$

and for the gas inside the bubble

$$\nabla\cdot\mathbf{u}=-\frac{1}{\rho}\frac{D\rho}{Dt}. \tag{3}$$

The bubble is assumed to consist of a noncondensable ideal gas going through an adiabatic process, i.e., $p\propto\rho^{\gamma}$, where γ is the ratio of specific heats. Heat transfer between the bubble and the liquid has been neglected; $\gamma=1.4$. The density variation can be related to pressure variation as follows:

$$\frac{1}{\rho}\frac{D\rho}{Dt}=\frac{1}{\gamma p}\frac{Dp}{Dt}, \tag{4}$$

D/Dt represent the Lagrangian derivative. Equation (4) is used in the numerical implementation of the continuity equation.[14]

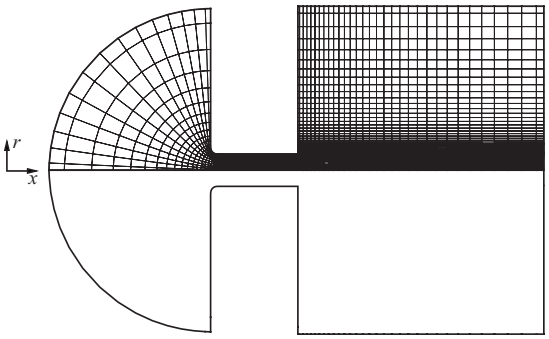

FIG. 1. Geometry of the axisymmetric orifice and the boundary-fitted grid. (Flow goes from left to right.)

III. NUMERICAL IMPLEMENTATION

The numerical solution of the unsteady Navier–Stokes equations is performed using the finite-volume method on a staggered grid. The SIMPLE algorithm[15] with QUICK discretization[16] of convective and advective terms is used.

In order to track the motion of the interface, the level-set[17,18] method is used. The level-set function θ is defined as a signed distance function from the interface with positive values on one side of the interface (gas phase) and negative values on the other side (liquid phase).

The level-set function is convected by the flow

$$\frac{\partial\theta}{\partial t}+\mathbf{u}\cdot\nabla\theta=0, \tag{5}$$

and the fluid properties are calculated as

$$\rho=\rho_l+(\rho_g-\rho_l)H_\epsilon(\theta), \tag{6}$$

$$\mu=\mu_l+(\mu_g-\mu_l)H_\epsilon(\theta), \tag{7}$$

where subscripts l,g correspond to liquid and gas, respectively. H_ϵ is a smoothed Heaviside function defined as

$$H_\epsilon=\begin{cases}0 & \theta<-\epsilon\\ (\theta+\epsilon)/(2\epsilon)+\sin(\pi\theta/\epsilon)/(2\pi) & |\theta|\le\epsilon\\ 1 & \theta>\epsilon,\end{cases} \tag{8}$$

where ϵ represents the half thickness of the interface and has been given the value of 1.5 times the grid spacing.

IV. ORIFICE FLOW SOLUTION

Cavitating flows in orifices have a wide range of time and length scales due to presence of micron size cavitation bubbles in the orifice. In order to overcome the difficulties of numerical simulation of such a system, the orifice flow has been decoupled from the bubble dynamics. In this approach, the orifice flow is solved first without bubbles and then the solution for pressure and shear in the orifice are used to create a similar environment for an individual cavitation bubble.

Figure 1 shows the orifice geometry and the computational domain in which the flow is solved. It is assumed that the flow remains axisymmetric and laminar. This is accurate since we are interested in the flow near the upstream corner of the orifice, where the flow is still laminar. Liquid at high

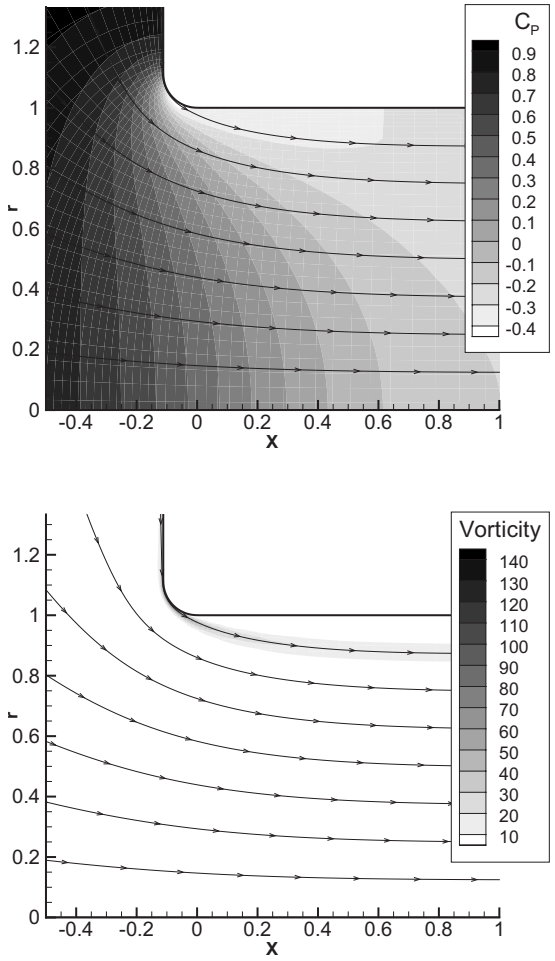

FIG. 2. Flow through an orifice at Re=8000: top, pressure coefficient and bottom, vorticity. The streamline that passes through the middle of the separated shear layer is used to find pressure history.

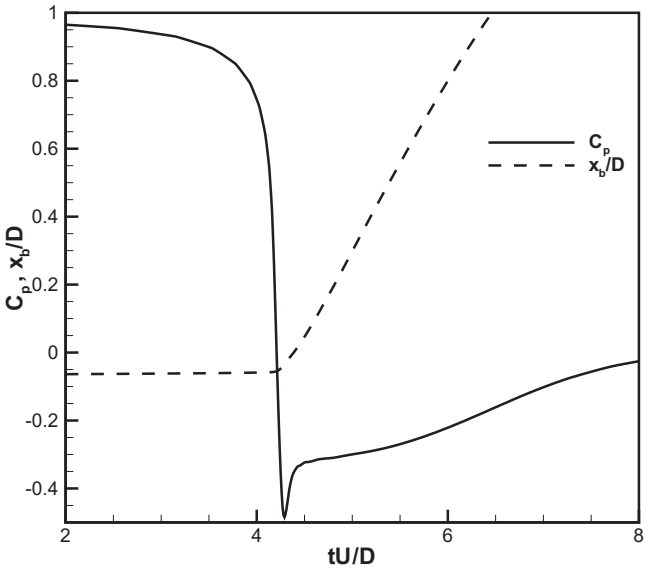

FIG. 3. History of the pressure coefficient C_p and the position of an element of mass along the orifice axis x_b. $C_p=P-P_d/\Delta P$.

pressure on the left in Fig. 1 flows through the orifice to the low-pressure ambient on right. No-slip boundary conditions are applied on the orifice wall and zero Lagrangian derivative is applied on the downstream boundary. Mass flux is specified on the upstream boundary. More details can be found in Dabiri *et al.*[10] The solution of the orifice flow is shown in Fig. 2. The calculation is performed for flow with a Reynolds number of Re=8000 based on the orifice diameter. A region of low pressure is present behind the inlet of the nozzle. This is where the cavitation inception will most likely occur. Looking at the vorticity contours, one can see that high levels of vorticity are also present at this point due to the boundary layer that separates from the nozzle wall downstream of the corner.

V. BUBBLE DYNAMICS IN ORIFICE FLOW

Now, we assume that any bubble in the flow will travel with the local velocity of the flow field. Therefore, by tracking a material point in the orifice one can find the pressure and shear rate that is felt by the particle. The particle path that has been chosen is the one that goes through the middle of the separated shear layer as shown in Fig. 2. Figure 3 shows the pressure history as an element of mass passes through the orifice along this path. The pressure drop occurs near the nozzle inlet and then the pressure recovers to the downstream pressure value. The pressure coefficient is defined as

$$C_p = \frac{P - P_d}{\Delta P}, \tag{9}$$

with P_d being the downstream pressure and ΔP the pressure drop across the orifice. This pressure profile then is applied as a time varying boundary condition for a bubble that grows and collapses in a shear flow or extensional flow. The computational domain consists of a cubic Cartesian grid with a simple shear flow, $u=k_s y$, or a two-dimensional extensional flow, $u=k_n x, v=-k_n y$. The magnitude of the shear rate or normal strain rate also comes from the orifice calculations. However, a constant strain rate is applied that does not vary with time and its value is the average value of the strain rate on the path of the bubble through the orifice. The bubble is initially spherical and is placed in the center of the computational domain. The frame of reference is attached to the center of mass of the bubble; so, the center of mass of the bubble does not move during the simulation. Moreover, considering the symmetry (about the $z=0$ plane) and antisymmetry (about the $y=0$ plane) in the problem, one needs to solve only a quarter of the domain, by applying correct boundary conditions.

Based on the governing Navier–Stokes equations, and the force balance at the interface, seven dimensionless parameters can be defined as follows:

$$\mathrm{Re} = \frac{\rho_l k R_o^2}{\mu_l}, \quad \mathrm{We} = \frac{\rho_l k^2 R_o^3}{\sigma}, \quad \alpha = kR_o\sqrt{\frac{\rho_l}{\Delta P}},$$
$$\beta = \frac{R_o}{D}, \quad K = \frac{\Delta P}{P_d}. \tag{10}$$

Two other dimensionless parameters are the liquid-to-gas density ratio and viscosity ratio each having an initial value

TABLE I. List of parameters for bubbles in orifice flow.

Case	Re	We	α	β	K	Flow type
Case 1	1.0	0.1	0.015 625	0.003 125	2.0142	Shear
Case 2	0.5	0.1	0.015 625	0.003 125	2.0142	Shear
Case 3	1.0	∞	0.015 625	0.003 125	2.0142	Shear
Case 4	0.5	∞	0.015 625	0.003 125	2.0142	Shear
Case 5	1.242	0.029 84	0.0352	0.004 405	2.5617	Shear
Case 6	0.621	0.007 461	0.017 62	0.004 405	2.5617	Shear

of 0.01. The viscosity of the gas is kept constant during simulation, but the density changes with time as the volume of the bubble varies. Reynolds and Weber numbers are defined based on the shear rate, k, initial radius of the bubble, R_o, and liquid properties. α defines the ratio of shear stress to the pressure drop across orifice, ΔP. β is the ratio of the bubble radius to the orifice diameter, D, and K is the ratio of the pressure drop across the orifice to the downstream pressure, P_d. Note that different and much larger Reynolds number and Weber number can be defined based on the orifice exit velocity corresponding to the pressure drop. The pressure drop across the orifice is of the same order of magnitude as the pressure difference across the liquid layer surrounding the bubble. Consequently, the normal velocity at the bubble surface will be of the same order as the orifice exit velocity. Based on the parameters that have been defined, the other Reynolds number will be Re/α and the Weber number will be We/α^2. More details on the governing equations and numerical method are provided in Ref. 14. Table I provides a list of parameters used in this study.

Figures 4–9 show snapshots of the cavitation bubble from the instant it reaches its maximum volume until it collapses and rebounds. Cross section of the bubble, velocity distribution and pressure contours are shown in each figure. Lengths are normalized by the initial radius of the bubble. The first image in Fig. 4 shows the bubble at its maximum volume. Due to liquid inertia, this maximum volume occurs slightly after the pressure reaches its minimum and starts to recover. At the maximum volume, the bubble has an ellipsoidal shape which is a result of the shear flow. As the bubble collapses, two regions of high-pressure are formed on upper right and lower left sides of the bubble. These high-pressure regions later lead to creation of two reentrant jets on both sides of the bubble. The formation of high-pressure regions and reentrant jets are similar to what has been observed during collapse of cavitation bubbles near rigid walls.[19] However, in that case only one reentrant jet is formed that collides with the other side of the bubble. On the other hand, the two reentrant jets, here, impinge on each other and create a liquid sheet. The impingement occurs at $t=1.315$, slightly after the bubble has reached its minimum volume at $t=1.302$. Then, the bubble rebounds and the impinging jets create a liquid sheet inside the bubble. In this case, the bubble remains integrated and does not break up into smaller bubbles.

The effects of viscosity have been studied by considering a lower Reynolds number in case 2. The results are shown in Fig. 5. The bubble at its maximum volume is very similar in shape to case 1. Also, during the collapse phase, the high-pressure regions near the sides of the bubble are observed. However, the reentrant jets are not as strong as before and they start to form later in time compared with case 1. In this case, the reentrant jets do not have enough momentum to overcome the viscous forces and they don't penetrate the bubble much and specifically they do not impinge on each other. Similar behavior is observed during collapse of cavitation bubbles near rigid walls by Popinet and Zalesky.[19] They found that the larger viscosity of the liquid prevents the reentrant jet to collide on the other side of the bubble.

Cases 3 and 4 are similar to cases 1 and 2, respectively, except that the surface tension is set to zero. The results are shown in Figs. 6 and 7. Comparing the results, one can find that the effects of surface tension are more pronounced for case 4 which has a lower Reynolds number. Even though the reentrant jets do not impinge in this case, similar to case 2, they penetrate much further into the bubble and almost reach each other. This can be explained by the fact that the lack of surface tension allows more deformation of the liquid-gas interface without any energy absorption.

Figure 8 shows case 5 which represents a higher surface tension coefficient and lower Weber number. Similarly, as the bubble collapses, the high-pressure regions and reentrant jets form on sides of the bubble. However, in this case, the jets are wider and have a size comparable to the size of the bubble itself. When the jets collide with each other, the bubble breaks up into two parts, while expanding in a direction normal to the shear flow. This high surface tension results in a capillary necking action which together with the reentrant jets lead to bubble fracture.

The independency of the results on the computational grid size has been checked by repeating the calculation for case 5 on a finer grid. The finer grid has 50% more nodes in each of x, y, and z directions. The maximum volume of the bubble calculated from the finer grid is only 5% different than the regular grid that has been used.

In case 6, both Reynolds number and Weber number have been reduced. As shown in Fig. 9, the collapse of the

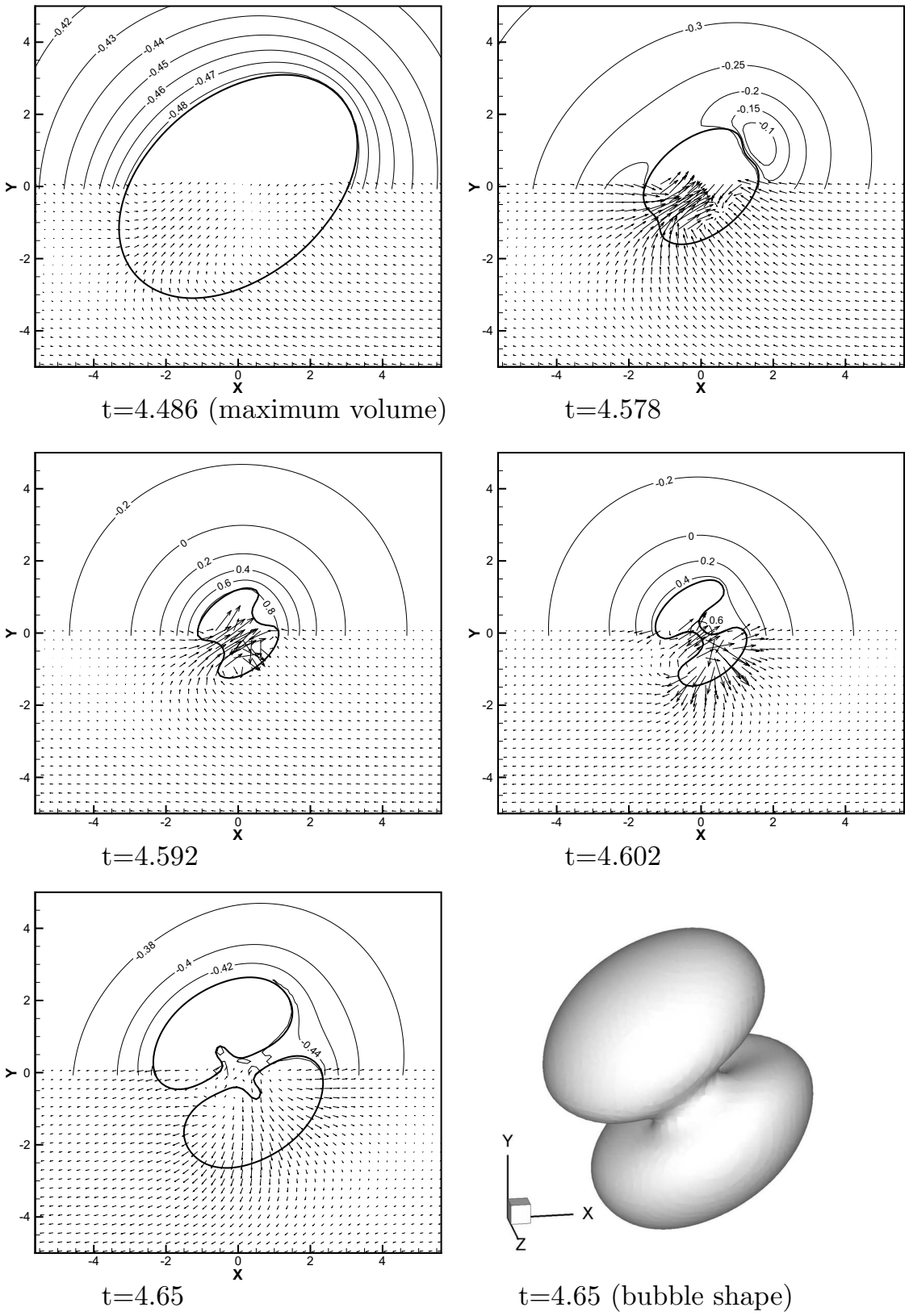

FIG. 4. Growth, collapse and rebound of cavitation bubble in shear flow for case 1, Re=1.0, We=0.1. Bubble interface, velocity vectors, and pressure coefficient contours are shown in the plane of symmetry of the bubble.

bubbles results in creation of a small satellite bubble in addition to the two main bubbles. However, the resolution of the computational domain is not high enough to resolve all the details of this satellite bubble.

A case with normal strain in the background flow is also studied. The background flow far from the bubble is a two dimensional stagnation point flow. Formation of reentrant jets is observed in this case as well.

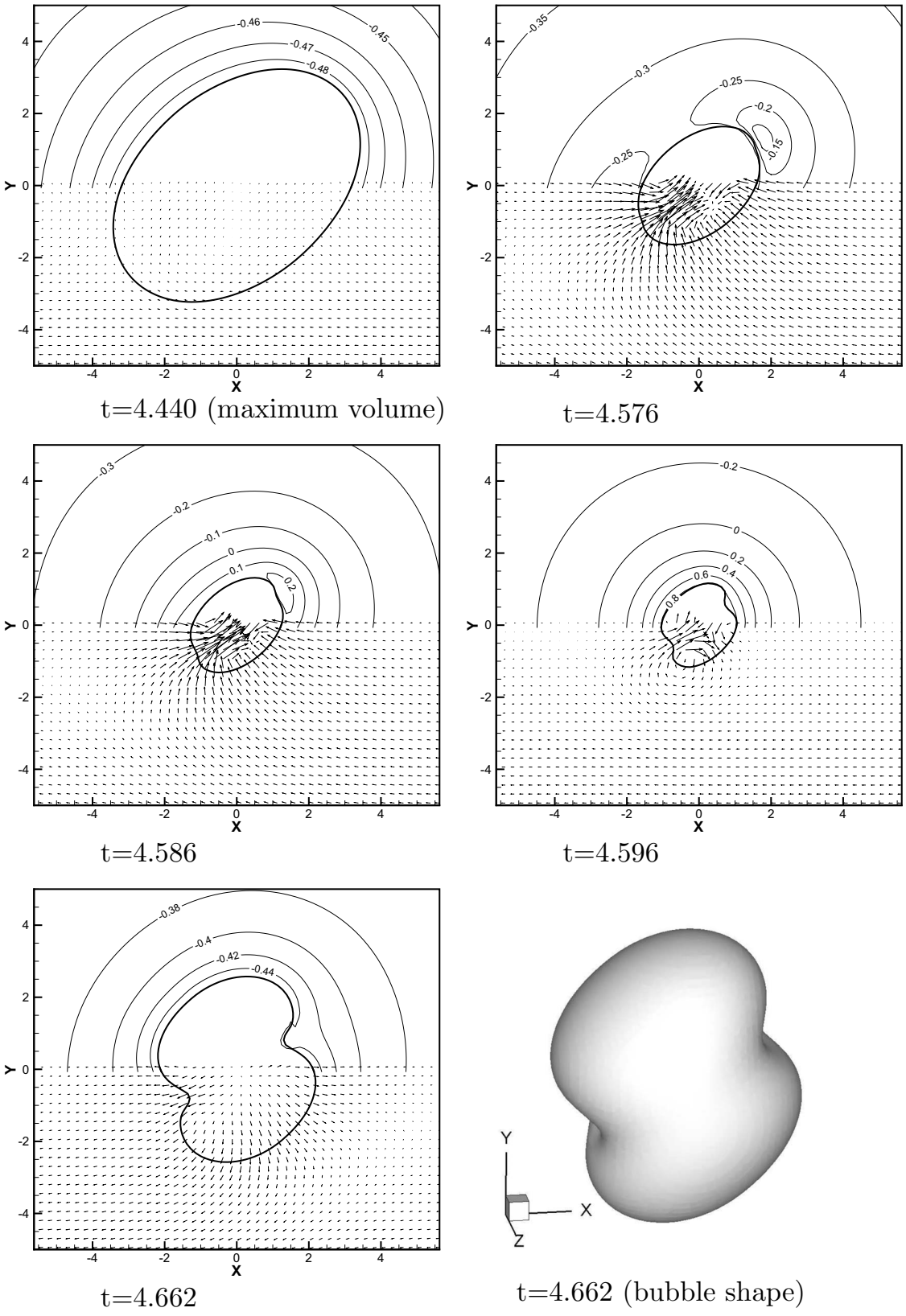

FIG. 5. Growth, collapse, and rebound of cavitation bubble in shear flow for case 2, Re=0.5, We=0.1. Bubble interface, velocity vectors, and pressure coefficient contours are shown in the plane of symmetry of the bubble.

VI. DISTURBANCES CAUSED BY CAVITATION

In this section, different types of disturbances in the flow that are created by cavitation bubbles are analyzed. These disturbances are the effects of monopole, quadrupole and vorticity generated during the growth and collapse of cavitation bubbles. The fluctuation in the velocity field due to these disturbances is evaluated at the orifice exit and compared to the average orifice flow velocity, U.

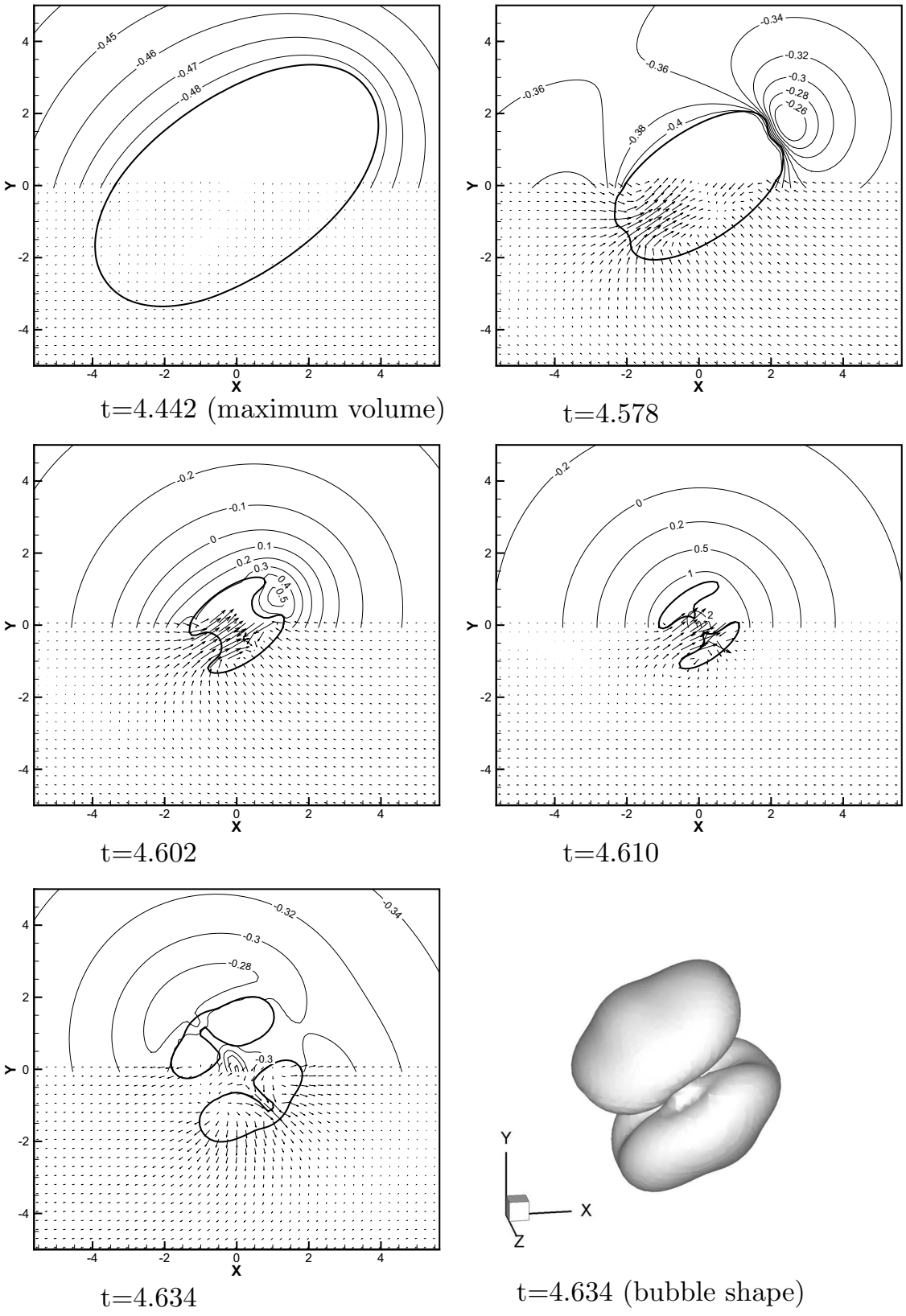

FIG. 6. Growth, collapse and rebound of cavitation bubble in shear flow for case 3, Re=1.0, We=∞. Bubble interface, velocity vectors, and pressure coefficient contours are shown in the plane of symmetry of the bubble.

The radial component of the velocity field around a bubble can be expanded in terms of spherical harmonics

$$u_r' = \sum_{n=0}^{\infty} \sum_{m=-n}^{n} A_n^m(r,t) Y_n^m(\theta,\phi), \tag{11}$$

$$= \sum_{n=0}^{\infty} \sum_{m=-n}^{n} \frac{q_n^m(t)}{r^{n+2}} Y_n^m(\theta,\phi), \tag{12}$$

where Y_n^m's are the spherical harmonics defined as

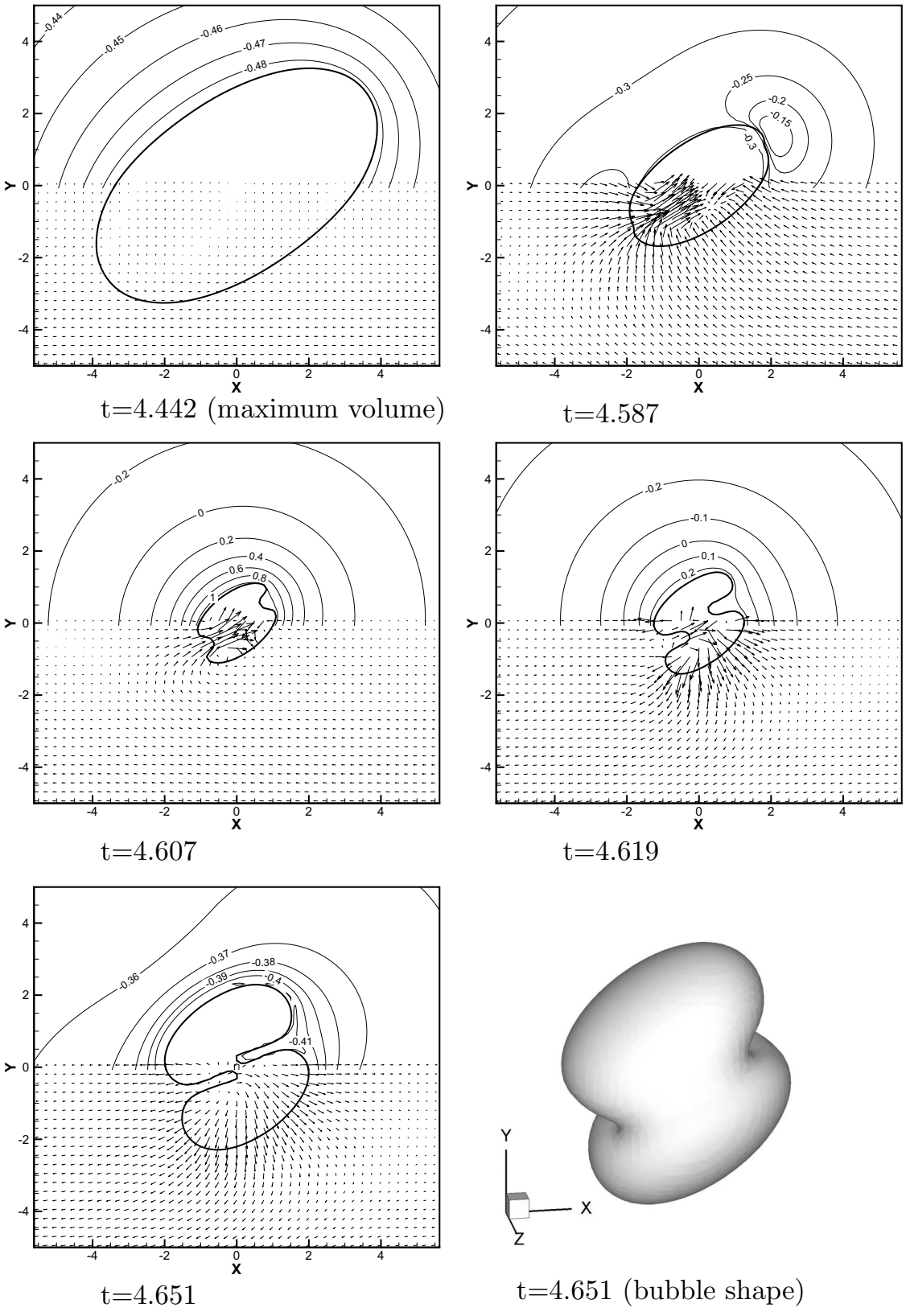

FIG. 7. Growth, collapse, and rebound of cavitation bubble in shear flow for case 4, Re=0.5, We=∞. Bubble interface, velocity vectors, and pressure coefficient contours are shown in the plane of symmetry of the bubble.

$$Y_n^m(\theta,\phi) = \sqrt{\frac{2n+1}{4\pi}\frac{(n-m)!}{(n+m)!}}P_n^m(\cos\,\theta)e^{im\phi}. \tag{13}$$

This representation is in spherical coordinates (r,θ,ϕ) with the origin at the center of the bubble. P_n^m are the Legendre polynomials and

$$\mathbf{u}' = \mathbf{u} - ky\hat{\mathbf{x}}. \tag{14}$$

A_n^m are the coefficients of the harmonics which are functions of time and radial distance r. Note that the exponent of r may

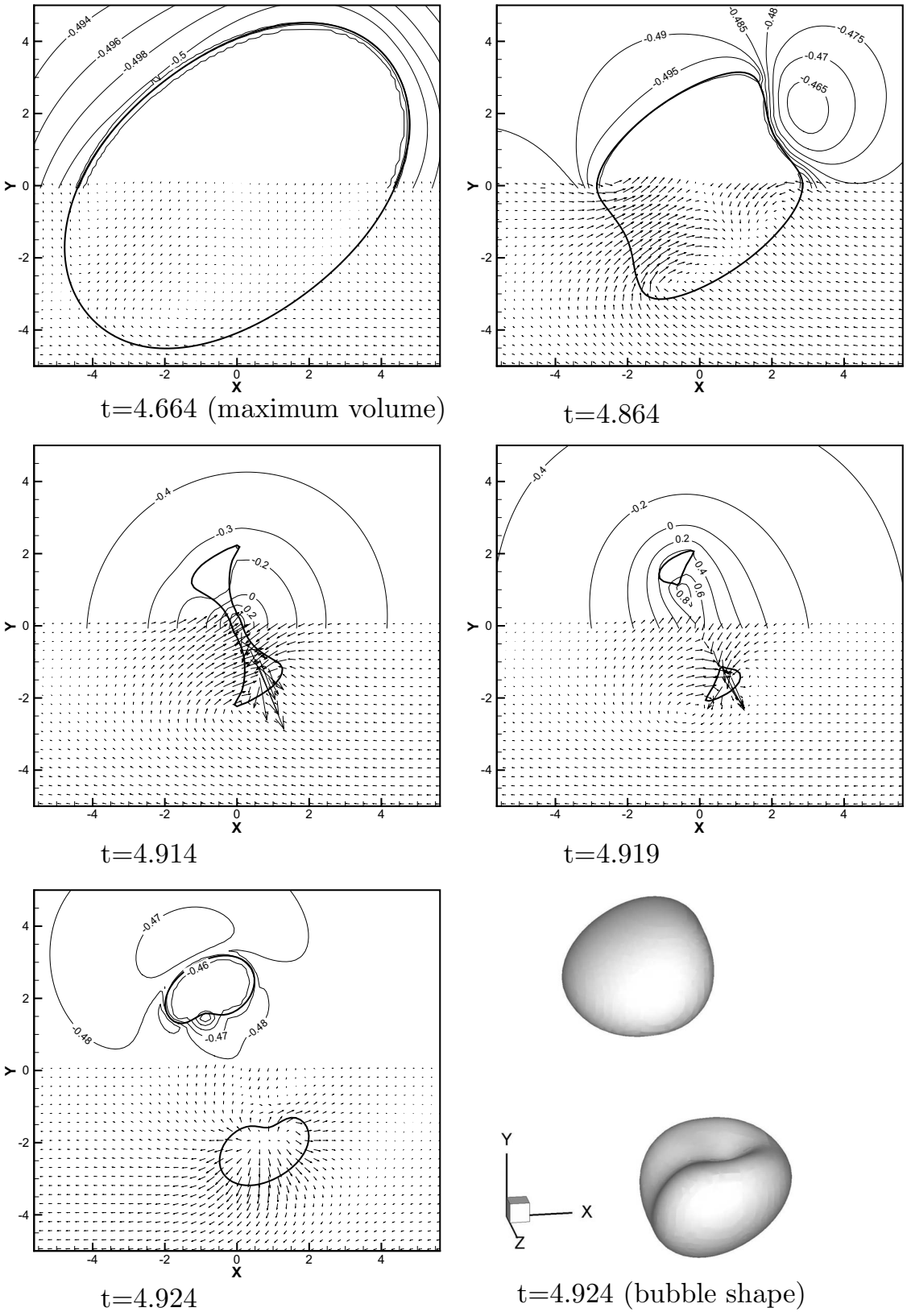

FIG. 8. Growth, collapse and rebound of cavitation bubble in shear flow for case 5, Re=1.242, We=0.029 84. Bubble interface, velocity vectors, and pressure coefficient contours are shown in the plane of symmetry of the bubble.

differ from the theoretical value of $n+2$ because the computational domain cannot be extended to infinite size while the monopole, quadrupole and other multipoles have a finite size. Equation (14) indicates that the background velocity has been subtracted from the velocity field before the spherical harmonics decomposition is performed. The time variation of the multipoles, q_n^m, are shown in Figs. 10 and 11.

The radial velocity component corresponding to the

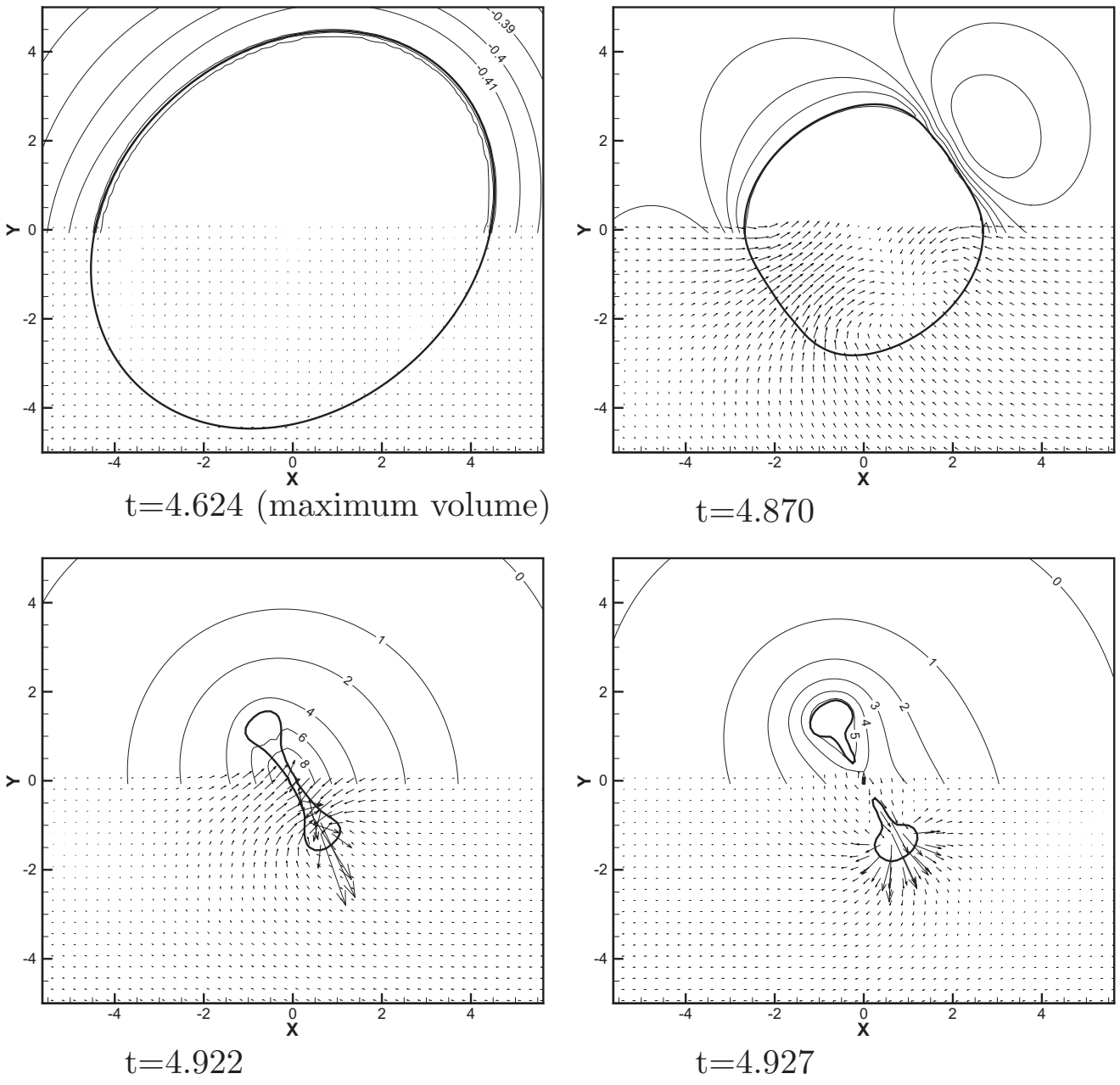

FIG. 9. Growth, collapse and rebound of cavitation bubble in shear flow for case 6, Re=0.621, We=0.007 461. Bubble interface, velocity vectors, and pressure coefficient contours are shown in the plane of symmetry of the bubble.

monopole source can be written as

$$u_r^\star = \frac{u_r}{R_o k} = \frac{1}{2\sqrt{\pi}} \frac{q_0^0}{(r/R_o)^2}, \tag{15}$$

and the rate of volume change can be related to the monopole

$$\frac{dV}{dt} = 4\pi r^2 u_r = 2\sqrt{\pi} R_o^3 k q_0^0. \tag{16}$$

If we assume that this volume change will propagate toward downstream and upstream of the bubble evenly, the velocity change caused by it at the orifice exit will be

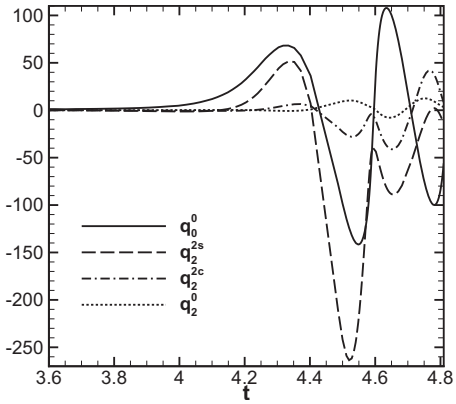

FIG. 10. Monopole and quadrupole moments for case 1.

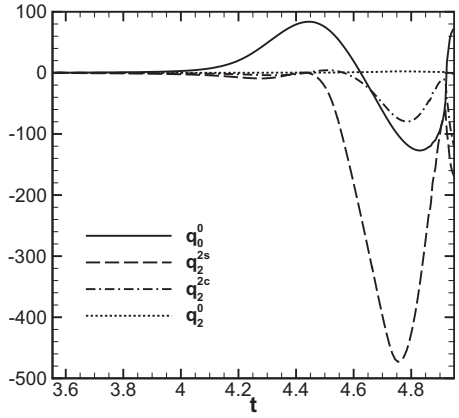

FIG. 11. Monopole and quadrupole moments for case 5.

$$\Delta U = \frac{1}{2}\frac{dV}{dt}\Big/\left(\frac{\pi}{4}D^2\right). \tag{17}$$

After normalizing with the orifice velocity, we find

$$\frac{\Delta U}{U} = \frac{4}{\sqrt{\pi}}\left(\frac{R_o}{D}\right)^2\left(\frac{kR_o}{U}\right)q_0^0. \tag{18}$$

Similarly, the quadrupole effect can be calculated as follows:

$$u_r^\star = \frac{u_r}{R_o k} = \frac{1}{4}\sqrt{\frac{15}{\pi}}\frac{q_2^2}{(r/R_o)^{3.5}}, \tag{19}$$

and then normalized by the average orifice velocity

$$\frac{\Delta U}{U} = \frac{1}{4}\sqrt{\frac{15}{\pi}}\left(\frac{R_o}{D}\right)^{3.5}\left(\frac{D}{L}\right)^{3.5}\left(\frac{kR_o}{U}\right)q_2^2. \tag{20}$$

The other candidate for increasing the disturbances in the flow during cavitation is the vorticity generated and advected in the flow. During the collapse of the bubble high vorticity regions are formed near the bubble surface. These vortices will remain in the liquid even after the bubble has collapsed, and will be convected downstream toward the exit. As the vortices travel, they become weaker due to viscous dissipation. Yet, they get closer to the orifice exit so could have more influence on the free-jet velocity. Here, we evaluate the strength of these velocity fields using some simple assumptions. During collapse of a single bubble, four regions of high vorticity are created which are roughly about an initial diameter of the bubble apart. A schematic of these vortices is shown in Fig. 12. To find the decay rate of these vortices, we approximate them by a Taylor–Green array of vortices.[20] Therefore, the vorticity at the center of each vortex can be written as

$$\omega = \omega_o e^{-\alpha t}, \tag{21}$$

where the decay rate, α, is

$$\alpha = 2\nu\left(\frac{2\pi}{\delta}\right)^2. \tag{22}$$

δ is the period of the vortex array in the Taylor–Green vortex which roughly has a value of $4R_o$ here. Assume that the vortices are created at the entrance of the orifice and then travel through it with average velocity of the flow. A schematic of orifice is shown in Fig. 13. The resident time of vortices inside the orifice is $\Delta t = L/U$, hence

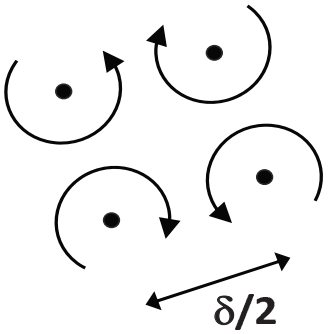

FIG. 12. Schematic of the vortices created during the collapse of bubble.

$$\alpha\Delta t = 2\nu\frac{4\pi^2}{16R_o^2}\frac{L}{D}. \tag{23}$$

Multiplying both numerator and denominator by D^2 and grouping the dimensionless parameters together, we have

$$\alpha\Delta t = \frac{\pi^2}{2}\frac{L}{D}\left(\frac{D}{R_o}\right)^2\frac{1}{\mathrm{Re}_D} = 101.9. \tag{24}$$

The velocity due to a vortex with uniform vorticity of ω in a region of radius R_o at a distance of r from the vortex is

$$u_v = \omega\frac{R_o^2}{r}. \tag{25}$$

Assume that, when the vortex exits the orifice, it has a distance of $D/10$ from the jet surface. The velocity imposed by vortex on the free surface is

$$\frac{u_v}{U} = \frac{\omega}{U}\frac{R_o^2}{D/10}. \tag{26}$$

The magnitude of ω_o comes from the simulation and it is of order of $100-1000k$. After substitution in the above equation, the normalized disturbance is found

$$\frac{u_v}{U} \simeq 10^4\left(\frac{R_o}{D}\right)\left(\frac{kR_o}{U}\right)\exp\left[-\frac{\pi^2}{2}\frac{L}{D}\left(\frac{D}{R_o}\right)^2\frac{1}{\mathrm{Re}_D}\right]. \tag{27}$$

Three equations (18), (20), and (27) are used to estimate the disturbances caused by each of the three mechanisms described here. Table II lists the relative disturbance in the free jet caused by these mechanisms. As can be seen, the

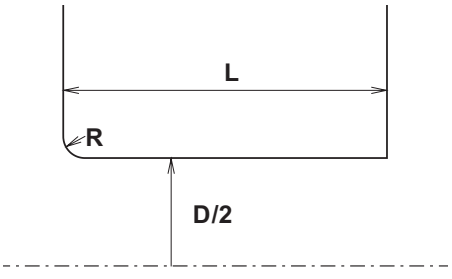

FIG. 13. Schematic of the orifice geometry

TABLE II. Relative strength of different types of disturbances caused by a single bubble in different cases.

Case	Monopole	Quadrupole	Advected vorticity
Case 1	6.91×10^{-5}	5.50×10^{-9}	2.56×10^{-28}
Case 2	6.72×10^{-5}	5.09×10^{-9}	2.56×10^{-28}
Case 3	7.79×10^{-5}	1.12×10^{-8}	2.56×10^{-28}
Case 5	2.77×10^{-4}	7.53×10^{-8}	3.44×10^{-14}
Case 6	2.80×10^{-4}	4.38×10^{-8}	1.72×10^{-14}

strongest disturbance is caused by the monopole source. The quadrupole is the next with four orders of magnitude smaller disturbances and advected vorticity is the last with six to nineteen orders of magnitude smaller than quadrupole effects. Note that these values represent the effect of a single cavitation bubble. Moreover, from Eq. (18), it can be seen that the magnitude of the disturbance is explicitly proportional to R_o^3 or the initial volume of the bubble. Hence, for a bubble with double the initial radius, the disturbances will be eight times larger. There is also an implicit dependency on R_o through the q_0^0, which is weak relative to the R_o^3 term. To investigate the dependency of q_0^0 on R_o, the Rayleigh–Plesset (RP) equations is solved for different initial radii. The RP equation[21] governs the radius of the bubble, R

$$R\ddot{R}+\frac{3}{2}\dot{R}^2=\frac{1}{\rho_l}\left\{P_g-P_\infty-\frac{2\sigma}{R}-\frac{4\mu_l}{R}\dot{R}\right\}, \tag{28}$$

where P_∞ is the pressure at infinity, P_g is the pressure inside the bubble at the interface and is related to the bubble volume through a polytropic equation $P_g=P_o(R_o/R)^{3\gamma}$, and P_o is the pressure inside the bubble at the initial equilibrium radius, R_o. The results are shown in Fig. 14. As it can be seen, while initial radius changes in a range of three orders of magnitude, q_0^0 varies only by a factor of 3.

The disturbances will grow in direct proportion to the number of bubbles in a neighborhood. Consequently, with the R_o^3 dependence, the disturbances will be proportional to the total bubble volume within this factor of 3 noted above.

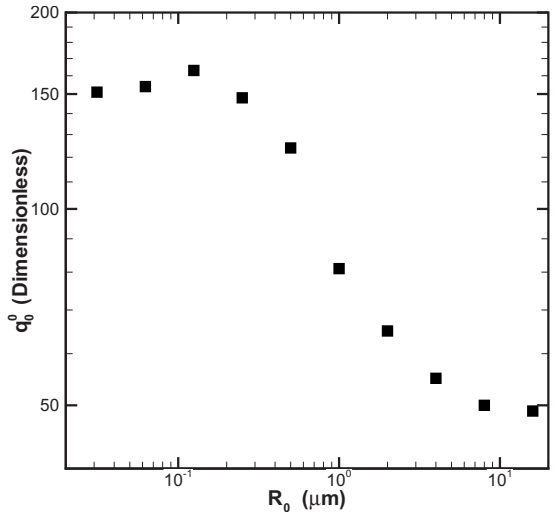

FIG. 14. Monopole strength as a function of initial radius of the bubble.

The total volume fraction of bubbles needed to obtain a 10% velocity fluctuation at the orifice exit is 4.6% for case 1.

A quantitative comparison cannot be made with the Giannadakis *et al.*[8] paper because of the significant differences in the orifice shape and Reynolds number. Qualitative similarities are found with the behavior of pressure and bubble size that are shown in their Fig. 4.

VII. CONCLUSIONS

The effects of cavitation on the orifice flow of an atomizer have been studied numerically by means of a one-way coupling between the orifice flow and cavitation bubbles. Navier–Stokes equation for two phase flows is solved to model growth and collapse of cavitation bubbles in the shear flow. A variable pressure boundary condition is imposed which is extracted from solution of viscous flow through an orifice. Reentrant jets are formed on the bubbles as they collapse. Impingement of these jets could result in break up of the cavitation bubble into two bubbles in some cases. Three mechanisms are suggested for increase in the disturbances in the flow and their effects have been estimated. These are monopoles, quadrupoles, and the vorticity generated during growth and collapse of bubbles. It is found that in the range of parameters studied here, the monopoles are the strongest source of disturbances at the orifice exit.

The cavitation models available in the literature[9,8] are based on spherical cavitation bubbles. The present work shows that the volume change of the bubble has the largest contribution to the disturbances generated by cavitation bubbles. This finding combined with the fact that the shear in the flow does not significantly affect the volume change of deformed cavitation bubbles, as shown by Dabiri *et al.*,[14] validates the use of models developed based on spherical bubbles. This work shows for a nonspherical bubble the dominance of the monopole term over the quadrupole and the vorticity-generation terms with regard to impact on the liquid flow. It has also been shown that the monopole source behaves exactly as it would for a spherical bubble of identical volume to the nonspherical bubble. So, in any two-way coupling, the treatment of the nonspherical bubble as a spherical bubble will be an excellent approximation. This analysis therefore provides a validation of existing two-way coupled computations that assumed spherical bubbles.

[1] N. Tamaki, M. Shimizu, and H. Hiroyasu, "Enhancement of the atomization of a liquid jet by cavitation in a nozzle hole," Atomization Sprays **11**, 125 (2001).
[2] H. Hiroyasu, "Spray breakup mechanism from the hole-type nozzle and its applications," Atomization Sprays **10**, 511 (2000).
[3] L. He and F. Ruiz, "Effect of cavitation on flow and turbulence in plain orifices for high-speed atomization," Atomization Sprays **5**, 569 (1995).
[4] C. Arcoumanis and M. Gavaises, "Linking nozzle flow with spray characteristics in a diesel fuel injection system," Atomization Sprays **8**, 307 (1998).
[5] C. Arcoumanis, M. Gavaises, and B. French, "Effect of fuel injection processes on the structure of diesel sprays," in SAE International Congress, February 1997, Detroit, Michigan, Paper 970799.
[6] A. Andriotis and M. Gavaises, "Influence of vortex flow and cavitation on near-nozzle diesel spray dispersion angle," Atomization Sprays **19**, 247 (2009).
[7] E. Giannadakis, D. Papoulias, M. Gavaises, C. Arcoumanis, C. Soteriou,

and W. Tang, "Evaluation of the predictive capability of diesel nozzle cavitation models," SAE Technical Paper Report No. 2007-01-0245, 2007.
[8]E. Giannadakis, M. Gavaises, and C. Arcoumanis, "Modelling of cavitation in diesel injector nozzles," J. Fluid Mech. **616**, 153 (2008).
[9]H. Y. A. Kubota and H. Kato, "A new modeling of cavitating flows: A numerical study of unsteady cavitation on a hydrofoil section," J. Fluid Mech. **240**, 59 (1992).
[10]S. Dabiri, W. A. Sirignano, and D. D. Joseph, "Cavitation in an orifice flow," Phys. Fluids **19**, 072112 (2007).
[11]S. Dabiri, W. A. Sirignano, and D. D. Joseph, "Two-dimensional and axisymmetric viscous flow in apertures," J. Fluid Mech. **605**, 1 (2008).
[12]P. W. Yu, L. Ceccio, and G. Tryggvason, "The collapse of a cavitation bubble in shear flows—A numerical study," Phys. Fluids **7**, 2608 (1995).
[13]P. A. Kottke, S. S. Bair, and W. O. Winer, "Cavitation in creeping shear flows," AIChE J. **51**, 2150 (2005).
[14]S. Dabiri, W. A. Sirignano, and D. D. Joseph, "Interaction between cavitation bubble and shear flow," J. Fluid Mech. (in press).
[15]S. V. Patankar, *Numerical Heat Transfer and Fluid Flow* (Hemisphere, Washington, DC, 1980).
[16]T. Hayase, J. A. C. Humphrey, and R. Greif, "A consistently formulated QUICK scheme for fast and stable convergence using finite-volume iterative calculation procedure," J. Comput. Phys. **98**, 108 (1992).
[17]M. Sussman, E. Fatemi, P. Smereka, and S. Osher, "An improved level set method for incompressible two-phase flows," Comput. Fluids **27**, 663 (1998).
[18]S. Osher and R. P. Fedkiw, "Level set methods: An overview and some recent results," J. Comput. Phys. **169**, 463 (2001).
[19]S. Popinet and S. Zaleski, "Bubble collapse near a solid boundary: A numerical study of the influence of viscosity," J. Fluid Mech. **464**, 137 (2002).
[20]G. I. Taylor and A. E. Green, "Mechanism of the production of small eddies from large ones," Proc. R. Soc. London, Ser. A **158**, 499 (1937).
[21]M. S. Plesset and A. Prosperetti, "Bubble dynamics and cavitation," Annu. Rev. Fluid Mech. **9**, 145 (1977).